

Article

Distinct Mechanisms of Target Search by Endonuclease VIII-like DNA Glycosylases

Evgeniia A. Diatlova¹, Grigory V. Mechetin¹ and Dmitry O. Zharkov^{1,2,*} 

¹ Siberian Branch of the Russian Academy of Sciences Institute of Chemical Biology and Fundamental Medicine, 8 Lavrentieva Ave., 630090 Novosibirsk, Russia

² Department of Natural Sciences, Novosibirsk State University, 2 Pirogova St., 630090 Novosibirsk, Russia

* Correspondence: dzharkov@niboch.nsc.ru

Abstract: Proteins that recognize specific DNA sequences or structural elements often find their cognate DNA lesions in a processive mode, in which an enzyme binds DNA non-specifically and then slides along the DNA contour by one-dimensional diffusion. Opposite to the processive mechanism is distributive search, when an enzyme binds, samples and releases DNA without significant lateral movement. Many DNA glycosylases, the repair enzymes that excise damaged bases from DNA, use processive search to find their cognate lesions. Here, using a method based on correlated cleavage of multiply damaged oligonucleotide substrates we investigate the mechanism of lesion search by three structurally related DNA glycosylases—bacterial endonuclease VIII (Nei) and its mammalian homologs NEIL1 and NEIL2. Similarly to another homologous enzyme, bacterial formamidopyrimidine–DNA glycosylase, NEIL1 seems to use a processive mode to locate its targets. However, the processivity of Nei was notably lower, and NEIL2 exhibited almost fully distributive action on all types of substrates. Although one-dimensional diffusion is often regarded as a universal search mechanism, our results indicate that even proteins sharing a common fold may be quite different in the ways they locate their targets in DNA.

Keywords: DNA repair; DNA glycosylases; endonuclease VIII; NEIL1; NEIL2; facilitated diffusion; target search



Citation: Diatlova, E.A.; Mechetin, G.V.; Zharkov, D.O. Distinct Mechanisms of Target Search by Endonuclease VIII-like DNA Glycosylases. *Cells* **2022**, *11*, 3192. <https://doi.org/10.3390/cells11203192>

Academic Editor: Inna N. Lavrik

Received: 14 September 2022

Accepted: 9 October 2022

Published: 11 October 2022

Publisher's Note: MDPI stays neutral with regard to jurisdictional claims in published maps and institutional affiliations.



Copyright: © 2022 by the authors. Licensee MDPI, Basel, Switzerland. This article is an open access article distributed under the terms and conditions of the Creative Commons Attribution (CC BY) license (<https://creativecommons.org/licenses/by/4.0/>).

1. Introduction

Many enzymes that recognize specific binding sites in DNA face the problem of finding them quickly and efficiently among a huge excess of competing non-specific DNA. This problem is relevant, in particular, for DNA repair enzymes, transcription factors, and restriction endonucleases [1]. To explain the mechanisms that allow proteins to scan DNA without energy costs, Berg and von Hippel in 1981 proposed four models: (i) sliding, in which the search is carried out by protein diffusion along the DNA chain in a random direction while the DNA–protein complex does not dissociate; (ii) hopping, when the protein moves between closely spaced sites of the DNA chain, always staying at a short distance from it, while the electrostatic interactions between the protein and the DNA are not completely lost; (iii) a distributive mechanism, involving multiple acts of association and dissociation of the DNA–protein complex; and (iv) intersegmental transfer of a protein molecule between sites distant along the DNA contour but accidentally close in space [2]. Sliding and hopping together constitute “facilitated diffusion”, or one-dimensional diffusion, often referred to as processive or correlated search mechanisms. The highest search rate is attained when proteins combine the processive and distributive search. The predominance of a particular mechanism depends on many factors that influence DNA–protein interactions, including the presence of mono- and divalent cations in the solvent shell, competition with other proteins for binding to DNA, etc. [3,4].

DNA repair enzymes target DNA lesions, which constantly appear in DNA due to the action of environmental (UV, ionizing radiation and chemical mutagens) and intracellular

(water, reactive oxygen and nitrogen species) damaging factors. This leads to modifications of nucleobases, formation of apurinic/apyrimidinic (AP) sites and single-strand breaks in DNA. Such lesions are usually repaired by the base excision repair system (BER). In the general BER pathway, common for both prokaryotes and eukaryotes, DNA glycosylases initiate the process by searching DNA, recognizing the damaged base and removing it through hydrolysis of the *N*-glycosidic bond between the base and the deoxyribose moiety [5]. AP endonucleases nick DNA at AP sites, either generated by DNA glycosylases or spontaneously formed. DNA polymerases then incorporate an appropriate undamaged nucleotide, or several nucleotides, the 5'-end is processed by a 2'-deoxyribo-5'-phosphate lyase or a flap endonuclease and the nick is sealed by a DNA ligase [5].

The main approaches for studying protein translocation can be divided into single-molecule (fluorescence microscopy or atomic force microscopy) and ensemble (kinetic assays). Several DNA glycosylases have been characterized with respect to their search mechanisms, including bacterial and human uracil–DNA glycosylases (Ung) [6–12] and mismatched adenine–DNA glycosylases MutY/MUTYH [13–15], human thymine–DNA glycosylase [16], alkylpurine–DNA glycosylase [17–19], 8-oxoguanine–DNA glycosylase [11,12,20–22], bacterial endonucleases III and VIII [23,24] and formamidopyrimidine–DNA glycosylase (Fpg) [13,14,20,21,23,24]. All of them employ, to a various degree, processive search, but different approaches sometimes give quantitatively discordant results, preventing a conclusive description of the search mechanisms.

Fpg and endonuclease VIII (Nei) are two homologous bacterial DNA glycosylases that remove oxidative lesions from DNA. Fpg is specific for damaged purine bases (8-oxoguanine and formamidopyrimidines), whereas Nei excises many oxidatively damaged pyrimidines [25,26]. In the early 2000s, three repair enzymes homologous to Nei were discovered in higher eukaryotes and named NEIL1 (Nei-Like 1), NEIL2 and NEIL3 [27–32]. Together with the plant homolog MMH, they form the helix–two-turn–helix (H2TH) structural superfamily characterized by the presence of the namesake DNA-binding motif. These enzymes repair oxidized bases but have overlapping substrate specificities with some other eukaryotic glycosylases (OGG1, NTHL1) and are not essential for the survival of the organism. Despite a number of studies characterizing their biochemistry, it is still an open question what is their main role in the cell. Thus far, it has been shown that NEIL1 interacts with some replication proteins, is up-regulated in the S phase and, therefore, likely repairs damaged bases in double-stranded (ds) DNA during replication [27,33–37]. NEIL2 prefers bubble structures and single-stranded (ss) DNA, interacts with RNA polymerase II and the transcriptional regulator heterogeneous nuclear ribonucleoprotein-U and has been suggested to repair DNA lesions during transcription [38–41]. NEIL3 shows preference for ssDNA and certain types of interstrand cross-links and likely has some specialized repair function [42–45].

Mechanisms of lesion search by Nei and NEILs remain poorly studied: diffusion constants for *Escherichia coli* Nei under different conditions were previously obtained using the single-molecule DNA tightrope assay [23,24], and the processivity of human NEIL1 was recently explored using kinetic analysis on a circular plasmid [46]. Here, using a biochemical processivity assay based on the cleavage of an oligonucleotide with two lesions [7,47], we have investigated the contribution of the facilitated diffusion into the lesion search by *E. coli* Nei and murine NEIL1 and NEIL2. Surprisingly, despite the structural similarity between Nei/NEIL1/NEIL2 and Fpg, the mechanisms supporting the processive search by these enzymes seem to be different.

2. Materials and Methods

2.1. Oligonucleotides and Substrate Preparation

Oligonucleotides were synthesized on an ASM-800 DNA/RNA Synthesizer (Biosset, Novosibirsk, Russia) from commercially available phosphoramidites (Glen Research, Sterling, VA, USA) and purified by electrophoresis in 8% or 20% polyacrylamide gel (PAGE) containing 8 M urea following by reverse-phase chromatography on NenSorb C18 sor-

bent (DuPont, Wilmington, DE, USA). The sequences of the oligonucleotides are listed in Table 1. When necessary, oligonucleotides were 5'-labeled using γ [32 P]-ATP (SB RAS ICBFM Laboratory of Biotechnology, Novosibirsk, Russia) and T4 polynucleotide kinase (Biosan, Novosibirsk, Russia) according to the manufacturer's protocol.

Table 1. Sequences of the oligonucleotides used in this work.

ID	Sequence (5' → 3') ^{a,b,c}
X1	TCCCTTCXCTCCTTTCCTTC
X2	GGACTTCXCTCCTTTCAGAG
C1	GAAGGAAAGGAGCGAAGGGA
C2	TCTGGAAAGGAGCGAAGTCC
comG	TCTGGAAAGGAGGGAAGTCCGAAGGAAAGGAGGGAAGGGA
X1+1	TCCCTTCXCTCCTTTCCTTC
comG+1	TCTGGAAAGGAGGGAAGTCCGGAAGGAAAGGAGGGAAGGGA
L40	pGGACTTTACTTTCGTTAGAGC
comG40	TCTGGAAAGGAGGGAAGTCCGCTCTAACGCAAGTAAAGTCCGAAGGAAAGGAGGGAAGGGA
L60	pGGACCTTTCAATTTGTGCGATCTTTCCTCTCGTTCAGACCTC
comG60(1)	pGATCGCACAAATGAAAGGTCCGAAGGAAAGGAGGGAAGGGA
comG60(2)	TCTGGAAAGGAGGGAAGTCCGAGGTCTGAACGAGAGGAAA
L80	pGGACCTTTCAATTTGTGCGATGAGTGAATTTCCGGATTTAGCTTTCCTCTCGTTCAGACCTC
comG80(1)	pAAATTCATCATCGCACAAATGAAAGGTCCGAAGGAAAGGAGGGAAGGGA
comG80(2)	TCTGGAAAGGAGGGAAGTCCGAGGTCTGAACGAGAGGAAAGCTAAATCCCC
comBub	TCTGGAAAGGAGATGGACTAACGAACCCAAGTAGAAGGGA
com30	AAAGGAGCGAAGTCCGAAGGAAAGGAGCGA

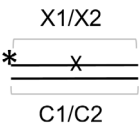
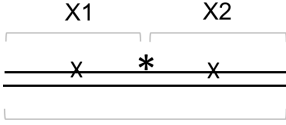
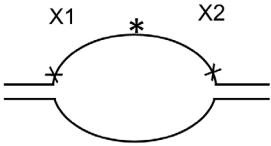
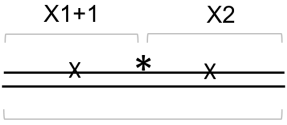
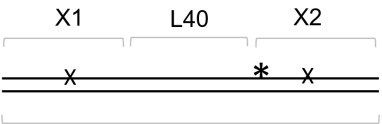
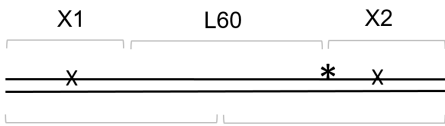

^a X, uracil (U) or 5-hydroxyuracil (OHU); ^b p, 5'-terminal phosphate introduced synthetically; ^c Bold underlined letters indicate the target base or the base complementary to it.

The general scheme of preparation substrates for the correlated cleavage assay was described previously [7,47]. The 40-mer ds substrates X1-X2//comG with two damaged bases were prepared by ligation of [32 P]-X2 with X1, both annealed to a 1.5-fold molar excess of the complementary 40-mer comG. The mixture was supplemented with T4 DNA ligase (New England Biolabs, Ipswich, MA, USA) and 2 mM ATP, and incubated overnight at 4 °C. The reaction product was purified by electrophoresis in 20% polyacrylamide gel containing 8 M urea and annealed to a 1.5-fold excess of the comG complementary strand.

The 40-mer ss substrate, X1-X2, was prepared similarly to the 40-mer ds substrate but with a 30-mer complementary strand com30 used for annealing to achieve complete separation of the scaffold strand during gel electrophoresis. To obtain the 40-mer bubble substrate, the purified ss 40-mer was annealed to the comBub complementary strand.

The 41-mer ds substrate with 20 bp between two damaged bases, (X1+1)-X2//comG+1, was prepared as above by annealing 5'-[32 P]-X2 with X1+1 and a 41-mer oligonucleotide scaffold comG+1. The 61-mer ds substrate with 40 bp between two lesions, X1-L40-X2//com40, was prepared by annealing [32 P]-X2, X1, and a 21-mer 5'-phosphorylated spacer L40 forming an intervening sequence between X1 and X2, with a 61-mer scaffold com40. The 81-mer ds substrate with 60 bp between two lesions, X1-L60-X2//comG60(1)-comG60(2), was prepared by annealing [32 P]-X2, X1 and a 41-mer 5'-phosphorylated spacer L60, with two scaffold oligonucleotides: a 5'-phosphorylated comG60(1) and non-phosphorylated comG60(2). The 101-mer ds substrate with 80 bp between two lesions, X1-L80-X2//comG80(1)-comG80(2), was prepared similarly with L80 as a spacer and comG80(1) and comG80(2), forming a ligation scaffold. The ligation was performed as described above, and the resulting 41-, 61-, 81- and 101-mer ds oligonucleotides were purified by electrophoresis in non-denaturing 8% polyacrylamide gel at 4 °C. Schematic representations of all substrates used in this work are shown in Table 2.

Table 2. Schemes of oligonucleotide substrates ^{a,b}.

Type of the Experiment			
Steady-state kinetics	Dependence on [K ⁺] and [Mg ²⁺]	Processivity of NEIL2	Dependence on the distance between the targets
 <p>C1/C2</p>	 <p>comG</p>	 <p>comBub</p>	 <p>comG+1</p>
			 <p>comG40</p>
			 <p>comG60(1) comG60(2)</p>
			 <p>comG80(1) comG80(2)</p>

^a See Table 1 for the IDs of the oligonucleotides used to construct the substrates. ^b Asterisk indicates the location of the [³²P] label. X indicates the damaged site.

2.2. Enzymes

Full-length murine NEIL1 and NEIL2 carrying a C-terminal His₆ tag were overexpressed and purified as described [32,48]. For purification of full-length, non-tagged *E. coli* Nei, the pET24b-Nei plasmid [49] was transformed into *E. coli* BL21(DE3) strain. The cells were grown in 2 L of the LB medium containing 100 µg/mL kanamycin at 37 °C to A₅₉₅ = 0.6 and induced with 1 mM isopropyl β-D-1-thiogalactopyranoside for 3 h. The cells were collected by centrifugation at 4 °C, resuspended in 40 mL of the lysis buffer (10 mM Tris-HCl (pH 8.0), 1 mM ethylenediaminetetraacetic acid (EDTA), 500 mM NaCl and 1 mM phenylmethylsulfonyl fluoride) and lysed by sonication. Cell debris was separated by centrifugation at 15,000× *g* for 20 min at 4 °C; then, the supernatant was treated with ammonium sulfate (80% saturation) for 2 h at 4 °C, and centrifuged again. The protein pellet was dissolved in 200 mL of Buffer A (25 mM HEPES-NaOH (pH 7.5), 1 mM EDTA and 1 mM dithiothreitol (DTT)) and the solution was passed through a 0.45 µm filter (Merck Millipore, Burlington, MA, USA), loaded onto a 25-mL SP Sepharose column (GE Healthcare, Chicago, IL, USA) and equilibrated in the same buffer. The bound protein was eluted with a gradient of 0–1000 mM NaCl in Buffer A. Fractions containing the target protein were identified by SDS-PAGE with Coomassie Blue staining. The fractions were diluted with Buffer A to ~50 mM NaCl, loaded onto a 5 mL HiTrap heparin Sepharose column (GE Healthcare), and the bound protein was eluted with a 25 mL gradient of 0–1000 mM NaCl in Buffer A. The fractions containing the target protein were dialyzed overnight against the buffer, containing 20 mM sodium phosphate (pH 7.5), 400 mM NaCl, 1 mM EDTA, 1 mM DTT and 50% glycerol, and stored at –20 °C.

2.3. Steady-State Kinetics

Kinetic parameters of Nei, NEIL1 and NEIL2 cleavage of 20-mer substrates X1/C1 and X2/C2 were obtained using AP sites as the lesions. To create AP sites, uracil-carrying substrates (100 pmol) were treated with 10 U of *E. coli* Ung (SibEnzyme, Novosibirsk, Russia) for 10 min at 37 °C immediately before use. The reaction mixture (10 µL) contained 20 mM Tris–HCl (pH 7.5), 1 mM EDTA, 1 mM DTT, 5–500 nM substrate and Nei (5 nM), NEIL1 (5 nM) or NEIL2 (10 nM). After 5 min at 37 °C, 5 µL of formamide-containing dye (80% formamide, 20 mM EDTA, 0.1% xylene cyanol and 0.1% bromophenol blue) was added, and the mixtures were heated for 2 min at 95 °C. The reaction products were resolved by 20% denaturing PAGE and visualized by phosphorimaging (Typhoon FLA 9500, GE Healthcare). The images were quantified using Quantity One v4.6.8 software (Bio-Rad Laboratories, Hercules, CA, USA). K_M and V_{max} were calculated by non-linear fitting to the Michaelis–Menten equation using SigmaPlot v11.0 (Systat Software, Frankfurt am Main, Germany).

2.4. Correlated Cleavage Assay

The correlated cleavage assay protocols were similar to the ones described in [7,47]. The concentrations of the substrates were taken in an excess, and the concentrations of the enzymes were optimized to operate in the nearly-linear part of product accumulation time courses. The reaction mixtures (25 µL) contained the appropriate 50 nM substrate, 20 mM Tris–HCl (pH 7.5), 1 mM EDTA, 1 mM DTT, 0–200 mM KCl and 0–20 mM MgCl₂. Reactions with NEIL2 on ss and bubble substrates did not contain salt. Dependence of cleavage by Nei and NEIL1 on the substrate length was studied at 25 mM KCl. The reactions were initiated by adding Nei (5 nM), NEIL1 (5 nM) or NEIL2 (10 nM) at 37 °C. At time points 0.5–10 min, aliquots (2.5 µL) were withdrawn, quenched with an equal volume of FDLB and heated for 2 min at 95 °C. The reaction products were resolved by 20% or 8% denaturing PAGE and visualized by phosphorimaging as above. The probability of correlated cleavage (P_{cc}) was calculated as $P_{cc} = v_{p3} / (v_{p1} + v_{p2} + v_{p3})$, where v_{p1} and v_{p2} are initial rates of accumulation of the products of cleavage at one of the sites and v_{p3} is the initial rate of accumulation of the double cleavage product.

2.5. Computational Analysis

Structure-assisted alignment of protein sequences was performed using Promals3D [50]. To calculate the electrostatic potential, DNA chains were removed from the structures of human NEIL1 (Protein Data Bank ID 5ITU [51]) and *E. coli* Nei (1K3W [52]), and the resulting protein structures were processed using PDB2PQR v3.5.2 and Adaptive Poisson–Boltzmann Solver (APBS v3.4.1) [53] at pH 7.5 and 0.01 M mobile charged ions (radius 2.0 Å). PyMol (Schrödinger, New York, NY, USA) was used for structural visualization and figure preparation.

3. Results

3.1. Steady-State Kinetics of Nei, NEIL1 and NEIL2 on Individual Target Sites

To study the processive search by Nei and NEILs, we have used a method based on measuring the probability of correlated cleavage of the oligonucleotide substrate containing two lesions [6,7,47]. When the substrate is in excess, full dissociation of the enzyme–product complex after the cleavage at one site makes re-association with the same substrate molecule a rare event, and double cleavage in the initial phase of the reaction reflects the processive transfer of the enzyme between the target sites (Figure 1a). A 40-mer substrate was obtained by ligating two 20-mers with the lesion embedded into identical DNA stretches in order to minimize sequence-dependent effects. To ensure that enzymes would recognize both targets equally well, Michaelis–Menten kinetics were performed on ds 20-mers (X1/C1 and X2/C2). Table 3 shows the kinetic parameters for 20-mers containing an AP site as a lesion universally recognized by Nei, NEIL1 and NEIL2. K_M and V_{max} of Nei and NEIL2 coincide for both substrates within the error margin. For NEIL1, enzyme saturation by the substrate

could not be achieved, and the V_{\max}/K_M ratio was determined instead of the individual K_M and V_{\max} values; the V_{\max}/K_M ratio was similar for both 20-mers. Thus, the interaction of Nei, NEIL1 and NEIL2 with both target sites is similar.

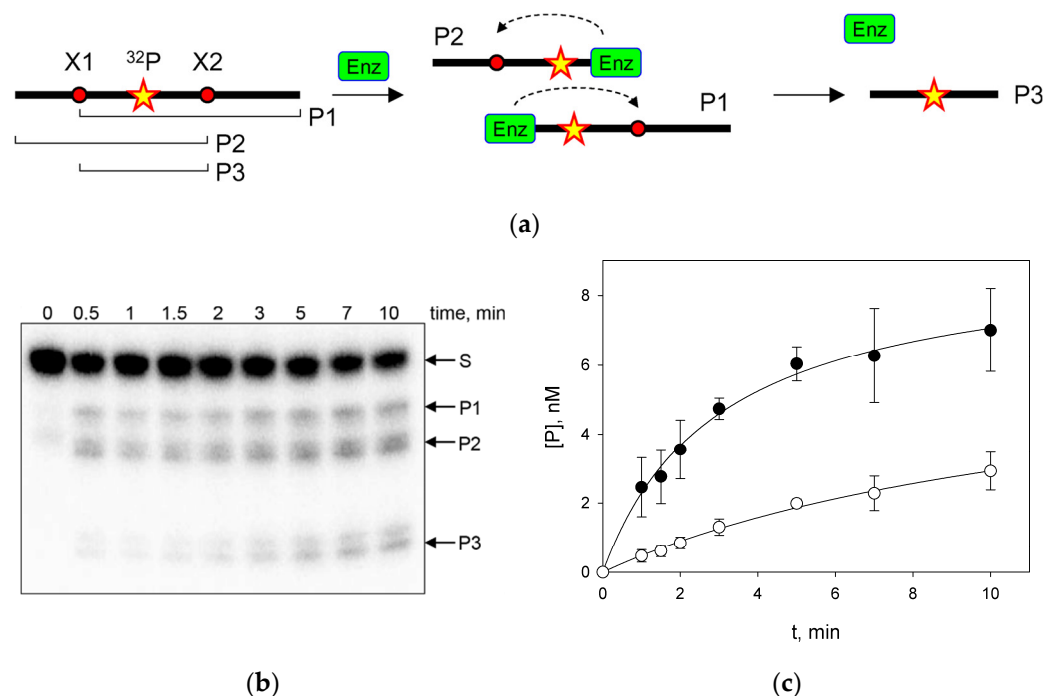


Figure 1. (a) General scheme of the correlated cleavage assay. Red dots indicate the damaged sites, star indicates a ^{32}P phosphate. (b) A representative gel showing the time course of a 40-mer substrate cleavage by Nei at 0 mM KCl. No enzyme was added at the 0 min time point. Arrows indicate positions of the 40-mer substrate and the products of different lengths (P1, 32-mer; P2, 27-mer; P3, 19-mer). (c) Time course of accumulation of P1 + P2 (black circles) and P3 (white circles) during the cleavage of a 40-mer substrate by Nei at 0 mM KCl. Mean \pm s.d. of four independent experiments are shown.

Table 3. Kinetic parameters of cleavage of double-stranded 20-mer oligonucleotides with an AP site by Nei, NEIL1 and NEIL2 ^a.

		K_M , nM	V_{\max} , nM \times min ⁻¹	V_{\max}/K_M , min ⁻¹
Nei	X1/C1	52 \pm 13	10 \pm 2	0.20 \pm 0.02
	X2/C2	56 \pm 17	11 \pm 2	0.20 \pm 0.02
NEIL1	X1/C1	n/d ^b	n/d	0.08 \pm 0.01
	X2/C2	n/d	n/d	0.12 \pm 0.01
NEIL2	X1/C1	101 \pm 22	17 \pm 3	0.17 \pm 0.01
	X2/C2	138 \pm 37	17 \pm 3	0.15 \pm 0.02

^a Mean \pm s.d. of two independent experiments; ^b n/d, not determined.

3.2. Correlated Cleavage of Substrates

To assess the processivity of Nei, NEIL1 and NEIL2, we used a substrate containing two 5-hydroxyuracil (OHU) residues. OHU is removed by these enzymes with different efficiencies [28,29,31,54] and is much more stable than the AP site thus facilitating preparation of the substrate and avoiding competition with Ung, which is used for AP site preparation in situ. The substrate is designed to produce bands of different mobility upon a single-hit cleavage at either damaged site. Two cleavage products at one of the sites (P1 and P2) and a cleavage product at both sites (P3) were easily observed (Figure 1b,c). From the ratio of the initial P3 accumulation rate to the total accumulation rate of all products, we calculated the

probability of correlated cleavage (P_{cc}), which, if the substrate is in excess, depends only on the nature of the studied enzyme, buffer composition and distance between lesions.

There are several factors that can affect the efficiency of facilitated diffusion, in particular, the presence of mono- and divalent metal ions in the medium [2–4]. DNA is always surrounded by a shell of counterions, with monovalent cations usually associated with the major DNA groove and interacting electrostatically, and Mg^{2+} cations forming coordination bonds in both grooves with backbone phosphates and with G in the major groove [55,56]. During diffusion of a protein along DNA, counterions must be displaced by the protein, which characteristically leads to a decrease in the diffusion constant with increasing ionic strength [2–4]. The dependence of the efficiency of protein translocation on the cation concentration is often used to prove that a protein searches for its target by one-dimensional scanning rather than in a distributive manner [3,57]. In particular, reduced one-dimensional search with increasing salt concentration was demonstrated for Fpg in both single-molecule and ensemble assays [13,20,21,23].

We have studied the effect of K^+ and Mg^{2+} cations on P_{cc} of Nei, NEIL1 and NEIL2 by varying the concentrations of KCl from 0 to 200 mM (Figure 2a) and $MgCl_2$ from 0 to 25 mM (Figure 2b). Quite unexpectedly, of all three enzymes, only NEIL1 was consistent with a processive search: its P_{cc} value reached 0.48 in the absence of cations other than Tris in the buffer, and decreased with increasing ion concentrations of K^+ or Mg^{2+} (Figure 2, blue plots). NEIL2 hardly used processive mechanisms, its P_{cc} values being about 0.1 over the entire range of cation concentrations (Figure 2, red plots). Nei behaved in an intermediate way, its P_{cc} values demonstrating a very shallow (but statistically significant) descent from 0.28 to 0.21 upon increasing KCl and largely insensitive to $MgCl_2$ (Figure 2, black plots). It is likely that such a profile indicates some features of the interaction of Nei and NEIL2 with DNA, indicating perhaps that their binding is mostly stabilized by non-electrostatic interactions, such as hydrophobic or van der Waals interactions. At 20 mM $MgCl_2$, P_{cc} increased noticeably for both Nei and NEIL2, which might be due to better stabilization of the duplex or the protein by Mg^{2+} ions. In general, the processivity of Nei, NEIL1 and NEIL2 was noticeably lower than that of the structurally related *E. coli* Fpg, for which, in exactly the same substrate system and reaction conditions, P_{cc} values up to 0.9 have been reported [21].

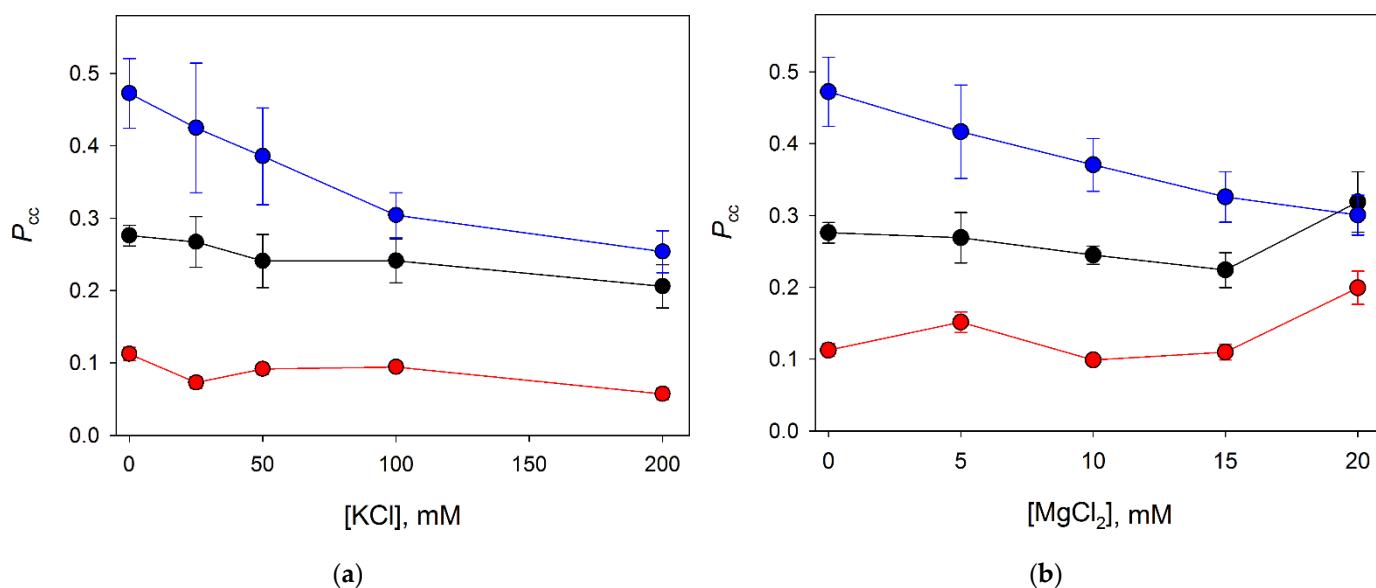


Figure 2. Effect of KCl (a) and $MgCl_2$ (b) on P_{cc} of Nei (black circles), NEIL1 (blue circles) and NEIL2 (red circles). Mean \pm s.d. of four independent experiments are shown.

3.3. Distance Dependence of the Correlated Cleavage

Processive target search in DNA is essentially a random walk with a finite probability of loss of the protein at each step [58]. Thus, the probability of correlated cleavage should decrease with longer distances between the lesion sites, as was shown for *E. coli* Ung [6,8,47]. To estimate how far Nei and NEIL1 can move in a processive manner along DNA before dissociation, we have determined P_{cc} on substrates where two OHU residues were separated by 20, 40, 60 or 80 bp. NEIL2 was not included because of its low processivity even at a short distance (see above). Much to our surprise, there was no noticeable decrease in the P_{cc} values over the entire range of intersite distances (Figure 3). In a recent report on the lesion search in plasmid substrates by human NEIL1, the estimated mean translocation distance was approximately 80 bp [46]. Given that NEIL1 here and in [46] showed a typical salt dependence profile, it is possible that NEIL1 is indeed processive and a decrease in P_{cc} would be observed at distances > 80 bp, which are not easily achieved in an oligonucleotide-based system. On the other hand, P_{cc} of Nei apparently did not depend on the intersite distance, which, together with weak salt dependence, is indicative of the low processivity of target search by this enzyme (see the Discussion for factors affecting the bulk processivity observed in double-cleavage experiments).

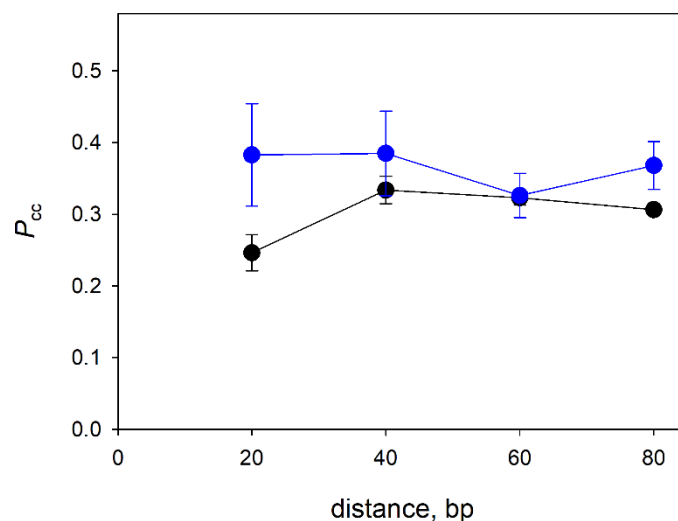


Figure 3. Dependence of P_{cc} of Nei (black circles) and NEIL1 (blue circles) on the distance between the damaged sites in the presence of 25 mM KCl. Mean \pm s.d. of three independent experiments are shown.

3.4. Processivity of NEIL2 on Substrates of Different Structure

Since dsDNA is not an optimal substrate for NEIL2, which prefers bubble and single-stranded substrates [38,41], we have inquired whether the correlated cleavage by NEIL2 may be higher in these alternative substrates. In the bubble substrate, the OHU residues were located at both ds/ss junctions of a 19-mer bubble; such substrates are efficiently processed by NEIL2 [41]. As can be seen in Figure 4, there was a tendency towards higher P_{cc} in the single-stranded substrate, which, however, did not reach statistical significance. No significant difference in P_{cc} was observed for the ds and bubble substrates. Together with the independence of P_{cc} on K^+ and Mg^{2+} concentrations and the overall low P_{cc} values, these findings strongly suggest that NEIL2 uses a distributive mechanism to search for its target sites in DNA.

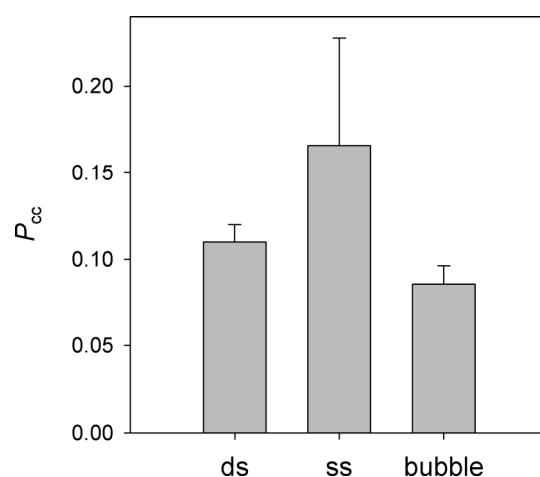


Figure 4. Correlated cleavage of double-stranded (ds), single-stranded (ss) and bubble DNA substrates by NEIL2. Mean \pm s.d. of three independent experiments are shown.

4. Discussion

Many proteins that recognize specific sequences, chemical modifications or structural elements in DNA, despite possessing quite different structural folds, share a common mechanism of target search, namely facilitated one-dimensional diffusion along the DNA contour. In particular, such a mechanism was demonstrated for a number of DNA glycosylases, the enzymes that recognize damaged nucleobases and initiate base excision DNA repair [6–24,46]. Here, we show that in a group of structurally related DNA glycosylases, all belonging to the same H2TH structural superfamily, may vary greatly in their ability to carry out processive lesion search, which, therefore, should not be taken for granted as a universal target location mechanism.

Together with this study, there are now four H2TH DNA glycosylases characterized to any extent with respect to the search mechanism: Fpg, Nei, NEIL1 and NEIL2 [13,14,20,21,23,24,46]. Fpg seems to be the most clear-cut case. In both ensemble [13,21] and single-molecule assays [14,20,23,24], Fpg from *E. coli* and *Geobacillus stearothermophilus* demonstrated considerable processivity. Single-molecule studies report the binding lifetime of Fpg at low salt in the 0.1 s–3.0 s range and the diffusion constant in the 3.5×10^5 bp²/s– 1.3×10^6 bp²/s range. This translates to an average displacement of 265 bp–2790 bp in a single binding event, consistent with very high P_{cc} (~0.9) observed in double-cleavage experiments [21]. At the other extreme is NEIL2, which, as we show here, is apparently almost fully distributive with dsDNA, ssDNA and bubble substrates. This is probably not surprising, as NEIL2 is known to be associated with the RNA polymerase II transcription complex [39,40,59], and thus, may not need to search for the lesions on its own, relying instead on a stalled polymerase for target recognition.

Rather unexpectedly, an increase in the distance between two target sites had almost no effect on P_{cc} of Nei and NEIL1. This is contrary to what was observed with Ung, which uses processive search surveying ~100 bp per binding event and shows correlated cleavage rapidly declining with distance [6,47]. However, NEIL1 demonstrated a typical salt dependence expected of processive search, with a significant fraction of correlated cleavage even at 200 mM KCl or 20 mM MgCl₂, whereas the correlated cleavage by Nei only modestly decreased from 0 to 200 mM KCl and was overall lower than the correlated cleavage by NEIL1. We suggest that this behavior may be explained in the framework of a model was proposed by Dunn et al. based on single-molecule “tightrope” experiments on target search in a high-molecular-weight λ phage DNA [23]. The model postulates that protein molecules searching for the target exist as at least two conformational populations: a slowly moving, tightly bound interrogation state, in which the protein probes whether the local properties of DNA correspond to its target, and a non-specific state, in which the protein rapidly slides and easily releases the bound DNA. If the populations are

interconverting slowly, P_{cc} values in the distance dependence experiment (Figure 3) would reflect the fraction of the enzyme molecules in the interrogation state with characteristic displacement distance considerably exceeding the largest intersite distance (80 bp in our case), while the others are rapidly falling off the DNA molecule. Consequently, ~40% of NEIL1 molecules and ~30% of Nei molecules would be in the interrogation state (Figure 3). Indeed, it is Ung that may be an exception from a common mechanism, since it recognizes uracil bases in spontaneously transiently opened base pairs [60,61], obviating the need for a dedicated interrogation state, whereas other DNA glycosylases, such as Fpg, have to force the target base pair opening [62–65].

Structural data available for Fpg, Nei, NEIL1 and MMH bound to DNA indicate that they all share similar overall organization of protein–DNA interactions [51,52,66–68]. The proteins possess an extensive, positively charged DNA-binding groove with a deep pocket, where the damaged base binds after being flipped out of the helix (Figure 5a–d). The H2TH motif and a β -hairpin zinc finger (or, in NEIL1 and MMH, an equivalent β -hairpin lacking a Zn^{2+} ion) bind backbone phosphates near the lesion and sharply kink the DNA axis facilitating the base flip-out. Although no structure of NEIL2 or NEIL3 bound to DNA is available, conservation of these basic elements in the structures of free NEIL2 from gray short-tailed opossum (*Monodelphis domestica*) [69], mouse NEIL3 [43] and the NEIL2/NEIL3-like protein from the giant Mimivirus [70] suggests that they bind DNA in a similar way. However, one prominent difference between Fpg/NEIL1/MMH on the one hand and Nei/NEIL2/NEIL3 on the other hand is the organization of a trio of amino acids that are inserted into the DNA helix to probe for damage and initiate the base eversion (Figure 5e). In Fpg, NEIL1 and MMH, they are absolutely conserved and include a methionine (Met80 in NEIL1) that fills the void left after base eversion, an arginine that recognizes the base opposite to the lesion (Arg117 in NEIL1) and a phenylalanine that wedges between the damaged base pair and the adjacent one to kink DNA (Phe119 in NEIL1). The Met residue comes from a loop between β_4 and β_5 strands in the N-terminal β -sandwich domain, whereas the Arg and Phe residues come from the β_7/β_8 loop (Figure 5a,e). In Nei, all three functionally equivalent residues (Leu, Gln and Tyr, respectively) come from the β_4/β_5 loop, and the β_7/β_8 loop is missing completely (Figure 5c,e). NEIL2 and NEIL3 retain, respectively, only two residues and one residue of the triad and also lack the β_7/β_8 loop, which likely reflects their preference for non-duplex DNA substrates. Nei, however, prefers ds substrates to ss and bubble substrates [41]. Nevertheless, the presence of a highly positively charged Arg residue in Fpg and NEIL1 right inside the DNA duplex could be one reason for tighter interaction and more pronounced salt sensitivity in comparison with the uncharged intercalating residues in Nei and NEIL2.

Yet another possibility is that overall lower Nei/NEIL2 processivity could be rooted in differences in the protein structural dynamics. H2TH proteins' catalytic core consists of two domains, N- and C-terminal, connected with a flexible linker. Regarding the orientation of their domains, Nei and NEIL2 proteins are shown to exist in two conformations, open and closed [52,69,71,72]. It is thought that free Nei and NEIL2 assume an open conformation and close upon DNA binding. Free NEIL1, however, exists in a closed conformation [73]. The structure of free *E. coli* Fpg is unknown; free Fpg from *Neisseria meningitidis* was crystallized in an open conformation [74], whereas free Fpg from *Thermus thermophilus* is closed [75]. Thus, Nei and NEIL2 could be intrinsically more prone to opening and DNA release than NEIL1 and Fpg.

In conclusion, regardless of the structural and mechanistic reasons underlying the differences in the processivity of H2TH superfamily DNA glycosylases, our results emphasize that DNA repair proteins, even those sharing a common fold, may be quite variable in the ways they use to search for their targets. Biologically, Fpg, NEIL1 and Nei likely act on their own to find DNA lesions, while NEIL2 most likely relies on an RNA polymerase as a damage sensor, which may explain its lower processivity as an isolated enzyme. Within the constraints imposed by their structure, proteins likely combine processive and distributive modes to achieve the most efficient search in the environment of the eukaryotic nucleus

or the bacterial nucleoid. Although there are very few examples of facilitated diffusion studied in living cells [76,77], only the development of suitable in situ assays will give an answer how well the mechanisms deduced from in vitro experiments align with the real kinetics of damage search by DNA repair enzymes.

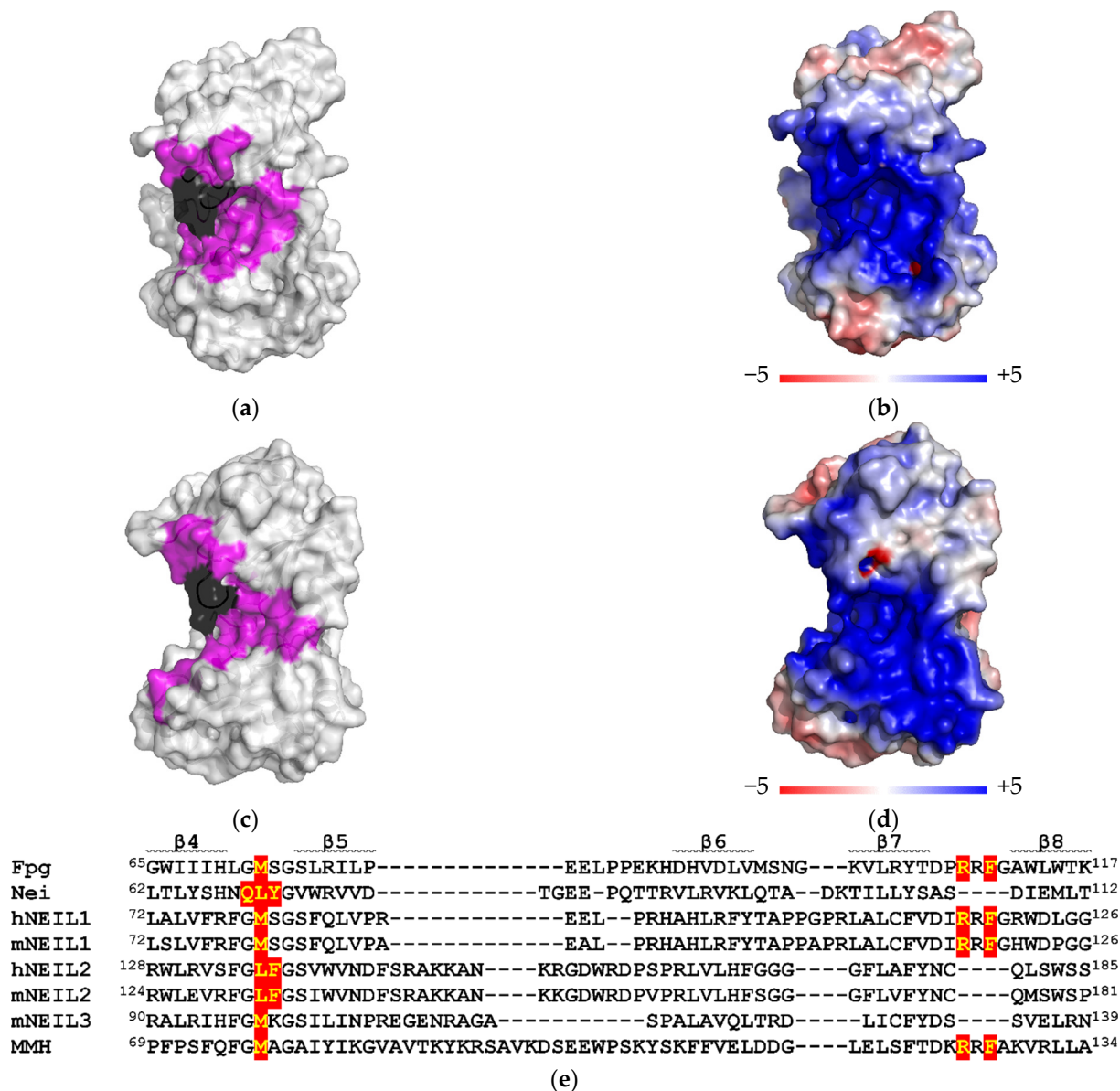


Figure 5. Structures of (a,b) NEIL1 (5ITU [51]) and (c,d) Nei (1K3W [52]). In (a,c), the DNA-binding groove defined as the residues within 4.0 Å from DNA is colored in magenta, and the intercalation triad is in black. In (b,d), the protein surface is colored according to the charge (blue, positive, red, negative; bar scale is in $k_B T/e_c$ units). (e), alignment of a part of the β -sandwich domain of H2TH superfamily proteins (*E. coli* Fpg, *E. coli* Nei, human NEIL1, mouse NEIL1, human NEIL2, mouse NEIL2, mouse NEIL3, *Arabidopsis thaliana* MMH) showing the intercalating triad in red.

Author Contributions: Conceptualization, D.O.Z.; methodology, E.A.D., G.V.M. and D.O.Z.; validation, E.A.D., G.V.M. and D.O.Z.; formal analysis, E.A.D.; investigation, E.A.D. and G.V.M.; resources, E.A.D., G.V.M. and D.O.Z.; data curation, E.A.D. and D.O.Z.; writing—original draft preparation, E.A.D.; writing—review and editing, D.O.Z.; visualization, E.A.D., G.V.M. and D.O.Z.; supervision, D.O.Z.; project administration, D.O.Z.; funding acquisition, D.O.Z. All authors have read and agreed to the published version of the manuscript.

Funding: This research was funded by the Russian Foundation for Basic Research (grant number 20-04-00554-a). Partial salary support from the Russian Ministry of Science and Higher Education (State funded budget project 121031300056-8 to D.O.Z.) is acknowledged.

Institutional Review Board Statement: Not applicable.

Informed Consent Statement: Not applicable.

Data Availability Statement: All data are contained in the paper.

Acknowledgments: We thank Maxim Kupryushkin (SB RAS ICBFM) for synthesis of the modified oligonucleotides.

Conflicts of Interest: The authors declare no conflict of interest. The funders had no role in the design of the study; in the collection, analyses or interpretation of data; in the writing of the manuscript; or in the decision to publish the results.

References

1. Zharkov, D.O.; Grollman, A.P. The DNA trackwalkers: Principles of lesion search and recognition by DNA glycosylases. *Mutat. Res.* **2005**, *577*, 24–54. [[CrossRef](#)] [[PubMed](#)]
2. Berg, O.G.; Winter, R.B.; von Hippel, P.H. Diffusion-driven mechanisms of protein translocation on nucleic acids. 1. Models and theory. *Biochemistry* **1981**, *20*, 6929–6948. [[CrossRef](#)] [[PubMed](#)]
3. Winter, R.B.; von Hippel, P.H. Diffusion-driven mechanisms of protein translocation on nucleic acids. 2. The *Escherichia coli* repressor–operator interaction: Equilibrium measurements. *Biochemistry* **1981**, *20*, 6948–6960. [[CrossRef](#)] [[PubMed](#)]
4. Winter, R.B.; Berg, O.G.; von Hippel, P.H. Diffusion-driven mechanisms of protein translocation on nucleic acids. 3. The *Escherichia coli lac* repressor–operator interaction: Kinetic measurements and conclusions. *Biochemistry* **1981**, *20*, 6961–6977. [[CrossRef](#)] [[PubMed](#)]
5. Friedberg, E.C.; Walker, G.C.; Siede, W.; Wood, R.D.; Schultz, R.A.; Ellenberger, T. *DNA Repair and Mutagenesis*; ASM Press: Washington, DC, USA, 2006; 1118p.
6. Porecha, R.H.; Stivers, J.T. Uracil DNA glycosylase uses DNA hopping and short-range sliding to trap extrahelical uracils. *Proc. Natl. Acad. Sci. USA* **2008**, *105*, 10791–10796. [[CrossRef](#)] [[PubMed](#)]
7. Sidorenko, V.S.; Mechetin, G.V.; Nevinsky, G.A.; Zharkov, D.O. Correlated cleavage of single- and double-stranded substrates by uracil-DNA glycosylase. *FEBS Lett.* **2008**, *582*, 410–414. [[CrossRef](#)]
8. Schonhoft, J.D.; Stivers, J.T. Timing facilitated site transfer of an enzyme on DNA. *Nat. Chem. Biol.* **2012**, *8*, 205–210. [[CrossRef](#)]
9. Schonhoft, J.D.; Kosowicz, J.G.; Stivers, J.T. DNA translocation by human uracil DNA glycosylase: Role of DNA phosphate charge. *Biochemistry* **2013**, *52*, 2526–2535. [[CrossRef](#)]
10. Schonhoft, J.D.; Stivers, J.T. DNA translocation by human uracil DNA glycosylase: The case of single-stranded DNA and clustered uracils. *Biochemistry* **2013**, *52*, 2536–2544. [[CrossRef](#)]
11. Cravens, S.L.; Schonhoft, J.D.; Rowland, M.M.; Rodriguez, A.A.; Anderson, B.G.; Stivers, J.T. Molecular crowding enhances facilitated diffusion of two human DNA glycosylases. *Nucleic Acids Res.* **2015**, *43*, 4087–4097. [[CrossRef](#)]
12. Cravens, S.L.; Stivers, J.T. Comparative effects of ions, molecular crowding, and bulk DNA on the damage search mechanisms of hOGG1 and hUNG. *Biochemistry* **2016**, *55*, 5230–5242. [[CrossRef](#)] [[PubMed](#)]
13. Francis, A.W.; David, S.S. *Escherichia coli* MutY and Fpg utilize a processive mechanism for target location. *Biochemistry* **2003**, *42*, 801–810. [[CrossRef](#)] [[PubMed](#)]
14. Blainey, P.C.; Luo, G.; Kou, S.C.; Mangel, W.F.; Verdine, G.L.; Bagchi, B.; Xie, X.S. Nonspecifically bound proteins spin while diffusing along DNA. *Nat. Struct. Mol. Biol.* **2009**, *16*, 1224–1229. [[CrossRef](#)] [[PubMed](#)]
15. Nelson, S.R.; Kathe, S.D.; Hilzinger, T.S.; Averill, A.M.; Warshaw, D.M.; Wallace, S.S.; Lee, A.J. Single molecule glycosylase studies with engineered 8-oxoguanine DNA damage sites show functional defects of a MUTYH polyposis variant. *Nucleic Acids Res.* **2019**, *47*, 3058–3071. [[CrossRef](#)]
16. Buechner, C.N.; Maiti, A.; Drohat, A.C.; Tessmer, I. Lesion search and recognition by thymine DNA glycosylase revealed by single molecule imaging. *Nucleic Acids Res.* **2015**, *43*, 2716–2729. [[CrossRef](#)]
17. Hedglin, M.; O'Brien, P.J. Human alkyladenine DNA glycosylase employs a processive search for DNA damage. *Biochemistry* **2008**, *47*, 11434–11445. [[CrossRef](#)]
18. Zhang, Y.; O'Brien, P.J. Repair of alkylation damage in eukaryotic chromatin depends on searching ability of alkyladenine DNA glycosylase. *ACS Chem. Biol.* **2015**, *10*, 2606–2615. [[CrossRef](#)]
19. Hendershot, J.M.; O'Brien, P.J. Search for DNA damage by human alkyladenine DNA glycosylase involves early intercalation by an aromatic residue. *J. Biol. Chem.* **2017**, *292*, 16070–16080. [[CrossRef](#)]
20. Blainey, P.C.; van Oijen, A.M.; Banerjee, A.; Verdine, G.L.; Xie, X.S. A base-excision DNA-repair protein finds intrahelical lesion bases by fast sliding in contact with DNA. *Proc. Natl. Acad. Sci. USA* **2006**, *103*, 5752–5757. [[CrossRef](#)]
21. Sidorenko, V.S.; Zharkov, D.O. Correlated cleavage of damaged DNA by bacterial and human 8-oxoguanine-DNA glycosylases. *Biochemistry* **2008**, *47*, 8970–8976. [[CrossRef](#)]

22. Rowland, M.M.; Schonhofs, J.D.; McKibbin, P.L.; David, S.S.; Stivers, J.T. Microscopic mechanism of DNA damage searching by hOGG1. *Nucleic Acids Res.* **2014**, *42*, 9295–9303. [[CrossRef](#)] [[PubMed](#)]
23. Dunn, A.R.; Kad, N.M.; Nelson, S.R.; Warshaw, D.M.; Wallace, S.S. Single Qdot-labeled glycosylase molecules use a wedge amino acid to probe for lesions while scanning along DNA. *Nucleic Acids Res.* **2011**, *39*, 7487–7498. [[CrossRef](#)] [[PubMed](#)]
24. Nelson, S.R.; Dunn, A.R.; Kathe, S.D.; Warshaw, D.M.; Wallace, S.S. Two glycosylase families diffusively scan DNA using a wedge residue to probe for and identify oxidatively damaged bases. *Proc. Natl. Acad. Sci. USA* **2014**, *111*, E2091–E2099. [[CrossRef](#)] [[PubMed](#)]
25. Zharkov, D.O.; Shoham, G.; Grollman, A.P. Structural characterization of the Fpg family of DNA glycosylases. *DNA Repair* **2003**, *2*, 839–862. [[CrossRef](#)]
26. Boiteux, S.; Coste, F.; Castaing, B. Repair of 8-oxo-7,8-dihydroguanine in prokaryotic and eukaryotic cells: Properties and biological roles of the Fpg and OGG1 DNA N-glycosylases. *Free Radic. Biol. Med.* **2017**, *107*, 179–201. [[CrossRef](#)]
27. Hazra, T.K.; Izumi, T.; Boldogh, I.; Imhoff, B.; Kow, Y.W.; Jaruga, P.; Dizdaroglu, M.; Mitra, S. Identification and characterization of a human DNA glycosylase for repair of modified bases in oxidatively damaged DNA. *Proc. Natl. Acad. Sci. USA* **2002**, *99*, 3523–3528. [[CrossRef](#)]
28. Bandaru, V.; Sunkara, S.; Wallace, S.S.; Bond, J.P. A novel human DNA glycosylase that removes oxidative DNA damage and is homologous to *Escherichia coli* endonuclease VIII. *DNA Repair* **2002**, *1*, 517–529. [[CrossRef](#)]
29. Hazra, T.K.; Kow, Y.W.; Hatahet, Z.; Imhoff, B.; Boldogh, I.; Mokkapatil, S.K.; Mitra, S.; Izumi, T. Identification and characterization of a novel human DNA glycosylase for repair of cytosine-derived lesions. *J. Biol. Chem.* **2002**, *277*, 30417–30420. [[CrossRef](#)]
30. Morland, I.; Rolseth, V.; Luna, L.; Rognes, T.; Bjørås, M.; Seeberg, E. Human DNA glycosylases of the bacterial Fpg/MutM superfamily: An alternative pathway for the repair of 8-oxoguanine and other oxidation products in DNA. *Nucleic Acids Res.* **2002**, *30*, 4926–4936. [[CrossRef](#)]
31. Takao, M.; Kanno, S.-i.; Kobayashi, K.; Zhang, Q.-M.; Yonei, S.; van der Horst, G.T.J.; Yasui, A. A back-up glycosylase in *Nth1* knock-out mice is a functional Nei (endonuclease VIII) homologue. *J. Biol. Chem.* **2002**, *277*, 42205–42213. [[CrossRef](#)]
32. Rosenquist, T.A.; Zaika, E.; Fernandes, A.S.; Zharkov, D.O.; Miller, H.; Grollman, A.P. The novel DNA glycosylase, NEIL1, protects mammalian cells from radiation-mediated cell death. *DNA Repair* **2003**, *2*, 581–591. [[CrossRef](#)]
33. Guan, X.; Bai, H.; Shi, G.; Theriot, C.A.; Hazra, T.K.; Mitra, S.; Lu, A.-L. The human checkpoint sensor Rad9–Rad1–Hus1 interacts with and stimulates NEIL1 glycosylase. *Nucleic Acids Res.* **2007**, *35*, 2463–2472. [[CrossRef](#)] [[PubMed](#)]
34. Dou, H.; Theriot, C.A.; Das, A.; Hegde, M.L.; Matsumoto, Y.; Boldogh, I.; Hazra, T.K.; Bhakat, K.K.; Mitra, S. Interaction of the human DNA glycosylase NEIL1 with proliferating cell nuclear antigen: The potential for replication-associated repair of oxidized bases in mammalian genomes. *J. Biol. Chem.* **2008**, *283*, 3130–3140. [[CrossRef](#)] [[PubMed](#)]
35. Theriot, C.A.; Hegde, M.L.; Hazra, T.K.; Mitra, S. RPA physically interacts with the human DNA glycosylase NEIL1 to regulate excision of oxidative DNA base damage in primer-template structures. *DNA Repair* **2010**, *9*, 643–652. [[CrossRef](#)]
36. Yamamoto, R.; Ohshiro, Y.; Shimotani, T.; Yamamoto, M.; Matsuyama, S.; Ide, H.; Kubo, K. Hypersensitivity of mouse NEIL1-knockdown cells to hydrogen peroxide during S phase. *J. Radiat. Res.* **2014**, *55*, 707–712. [[CrossRef](#)]
37. Albelazi, M.S.; Martin, P.R.; Mohammed, S.; Mutti, L.; Parsons, J.L.; Elder, R.H. The biochemical role of the human NEIL1 and NEIL3 DNA glycosylases on model DNA replication forks. *Genes* **2019**, *10*, 315. [[CrossRef](#)]
38. Dou, H.; Mitra, S.; Hazra, T.K. Repair of oxidized bases in DNA bubble structures by human DNA glycosylases NEIL1 and NEIL2. *J. Biol. Chem.* **2003**, *278*, 49679–49684. [[CrossRef](#)]
39. Banerjee, D.; Mandal, S.M.; Das, A.; Hegde, M.L.; Das, S.; Bhakat, K.K.; Boldogh, I.; Sarkar, P.S.; Mitra, S.; Hazra, T.K. Preferential repair of oxidized base damage in the transcribed genes of mammalian cells. *J. Biol. Chem.* **2011**, *286*, 6006–6016. [[CrossRef](#)]
40. Chakraborty, A.; Wakamiya, M.; Venkova-Canova, T.; Pandita, R.K.; Aguilera-Aguirre, L.; Sarker, A.H.; Singh, D.K.; Hosoki, K.; Wood, T.G.; Sharma, G.; et al. *Neil2*-null mice accumulate oxidized DNA bases in the transcriptionally active sequences of the genome and are susceptible to innate inflammation. *J. Biol. Chem.* **2015**, *290*, 24636–24648. [[CrossRef](#)]
41. Makasheva, K.A.; Endutkin, A.V.; Zharkov, D.O. Requirements for DNA bubble structure for efficient cleavage by helix–two-turn–helix DNA glycosylases. *Mutagenesis* **2020**, *35*, 119–128. [[CrossRef](#)]
42. Liu, M.; Bandaru, V.; Bond, J.P.; Jaruga, P.; Zhao, X.; Christov, P.P.; Burrows, C.J.; Rizzo, C.J.; Dizdaroglu, M.; Wallace, S.S. The mouse ortholog of NEIL3 is a functional DNA glycosylase in vitro and in vivo. *Proc. Natl. Acad. Sci. USA* **2010**, *107*, 4925–4930. [[CrossRef](#)] [[PubMed](#)]
43. Liu, M.; Imamura, K.; Averill, A.M.; Wallace, S.S.; Doublé, S. Structural characterization of a mouse ortholog of human NEIL3 with a marked preference for single-stranded DNA. *Structure* **2013**, *21*, 247–256. [[CrossRef](#)] [[PubMed](#)]
44. Semlow, D.R.; Zhang, J.; Budzowska, M.; Drohat, A.C.; Walter, J.C. Replication-dependent unhooking of DNA interstrand cross-links by the NEIL3 glycosylase. *Cell* **2016**, *167*, 498–511.e414. [[CrossRef](#)] [[PubMed](#)]
45. Martin, P.R.; Couvé, S.; Zutterling, C.; Albelazi, M.S.; Groisman, R.; Matkarimov, B.T.; Parsons, J.L.; Elder, R.H.; Saparbaev, M.K. The human DNA glycosylases NEIL1 and NEIL3 excise psoralen-induced DNA-DNA cross-links in a four-stranded DNA structure. *Sci. Rep.* **2017**, *7*, 17438. [[CrossRef](#)]
46. Kolbanovskiy, M.; Aharonoff, A.; Sales, A.H.; Geacintov, N.E.; Shafirovich, V. Recognition and repair of oxidatively generated DNA lesions in plasmid DNA by a facilitated diffusion mechanism. *Biochem. J.* **2021**, *478*, 2359–2370. [[CrossRef](#)] [[PubMed](#)]
47. Mechetin, G.V.; Zharkov, D.O. Mechanism of translocation of uracil-DNA glycosylase from *Escherichia coli* between distributed lesions. *Biochem. Biophys. Res. Commun.* **2011**, *414*, 425–430. [[CrossRef](#)]

48. Conlon, K.A.; Miller, H.; Rosenquist, T.A.; Zharkov, D.O.; Berrios, M. The murine DNA glycosylase NEIL2 (mNEIL2) and human DNA polymerase β bind microtubules in situ and in vitro. *DNA Repair* **2005**, *4*, 419–431. [[CrossRef](#)]
49. Rieger, R.A.; McTigue, M.M.; Kycia, J.H.; Gerchman, S.E.; Grollman, A.P.; Iden, C.R. Characterization of a cross-linked DNA-endonuclease VIII repair complex by electrospray ionization mass spectrometry. *J. Am. Soc. Mass Spectrom.* **2000**, *11*, 505–515. [[CrossRef](#)]
50. Pei, J.; Kim, B.-H.; Grishin, N.V. PROMALS3D: A tool for multiple protein sequence and structure alignments. *Nucleic Acids Res.* **2008**, *36*, 2295–2300. [[CrossRef](#)]
51. Zhu, C.; Lu, L.; Zhang, J.; Yue, Z.; Song, J.; Zong, S.; Liu, M.; Stovicek, O.; Gao, Y.Q.; Yi, C. Tautomerization-dependent recognition and excision of oxidation damage in base-excision DNA repair. *Proc. Natl. Acad. Sci. USA* **2016**, *113*, 7792–7797. [[CrossRef](#)]
52. Zharkov, D.O.; Golan, G.; Gilboa, R.; Fernandes, A.S.; Gerchman, S.E.; Kycia, J.H.; Rieger, R.A.; Grollman, A.P.; Shoham, G. Structural analysis of an *Escherichia coli* endonuclease VIII covalent reaction intermediate. *EMBO J.* **2002**, *21*, 789–800. [[CrossRef](#)] [[PubMed](#)]
53. Jurrus, E.; Engel, D.; Star, K.; Monson, K.; Brandi, J.; Felberg, L.E.; Brookes, D.H.; Wilson, L.; Chen, J.; Liles, K.; et al. Improvements to the APBS biomolecular solvation software suite. *Protein Sci.* **2018**, *27*, 112–128. [[CrossRef](#)] [[PubMed](#)]
54. Jiang, D.; Hatahet, Z.; Melamed, R.J.; Kow, Y.W.; Wallace, S.S. Characterization of *Escherichia coli* endonuclease VIII. *J. Biol. Chem.* **1997**, *272*, 32230–32239. [[CrossRef](#)] [[PubMed](#)]
55. Bonvin, A.M.J.J. Localisation and dynamics of sodium counterions around DNA in solution from molecular dynamics simulation. *Eur. Biophys. J.* **2000**, *29*, 57–60. [[CrossRef](#)] [[PubMed](#)]
56. Subirana, J.A.; Soler-López, M. Cations as hydrogen bond donors: A view of electrostatic interactions in DNA. *Annu. Rev. Biophys. Biomol. Struct.* **2003**, *32*, 27–45. [[CrossRef](#)] [[PubMed](#)]
57. Stanford, N.P.; Szczelkun, M.D.; Marko, J.F.; Halford, S.E. One- and three-dimensional pathways for proteins to reach specific DNA sites. *EMBO J.* **2000**, *19*, 6546–6557. [[CrossRef](#)]
58. Belotserkovskii, B.P.; Zarlino, D.A. Analysis of a one-dimensional random walk with irreversible losses at each step: Applications for protein movement on DNA. *J. Theor. Biol.* **2004**, *226*, 195–203. [[CrossRef](#)]
59. Aamann, M.D.; Hvitby, C.; Popuri, V.; Muftuoglu, M.; Lemminger, L.; Skeby, C.K.; Keijzers, G.; Ahn, B.; Bjørås, M.; Bohr, V.A.; et al. Cockayne Syndrome group B protein stimulates NEIL2 DNA glycosylase activity. *Mech. Ageing Dev.* **2014**, *135*, 1–14. [[CrossRef](#)]
60. Cao, C.; Jiang, Y.L.; Stivers, J.T.; Song, F. Dynamic opening of DNA during the enzymatic search for a damaged base. *Nat. Struct. Mol. Biol.* **2004**, *11*, 1230–1236. [[CrossRef](#)]
61. Parker, J.B.; Bianchet, M.A.; Krosky, D.J.; Friedman, J.I.; Amzel, L.M.; Stivers, J.T. Enzymatic capture of an extrahelical thymine in the search for uracil in DNA. *Nature* **2007**, *449*, 433–437. [[CrossRef](#)]
62. Banerjee, A.; Santos, W.L.; Verdine, G.L. Structure of a DNA glycosylase searching for lesions. *Science* **2006**, *311*, 1153–1157. [[CrossRef](#)] [[PubMed](#)]
63. Qi, Y.; Spong, M.C.; Nam, K.; Banerjee, A.; Jiralerspong, S.; Karplus, M.; Verdine, G.L. Encounter and extrusion of an intrahelical lesion by a DNA repair enzyme. *Nature* **2009**, *462*, 762–766. [[CrossRef](#)] [[PubMed](#)]
64. Kuznetsov, N.A.; Bergonzo, C.; Campbell, A.J.; Li, H.; Mechetin, G.V.; de los Santos, C.; Grollman, A.P.; Fedorova, O.S.; Zharkov, D.O.; Simmerling, C. Active destabilization of base pairs by a DNA glycosylase wedge initiates damage recognition. *Nucleic Acids Res.* **2015**, *43*, 272–281. [[CrossRef](#)] [[PubMed](#)]
65. Li, H.; Endutkin, A.V.; Bergonzo, C.; Campbell, A.J.; de los Santos, C.; Grollman, A.; Zharkov, D.O.; Simmerling, C. A dynamic checkpoint in oxidative lesion discrimination by formamidopyrimidine–DNA glycosylase. *Nucleic Acids Res.* **2016**, *44*, 683–694. [[CrossRef](#)]
66. Fromme, J.C.; Verdine, G.L. Structural insights into lesion recognition and repair by the bacterial 8-oxoguanine DNA glycosylase MutM. *Nat. Struct. Biol.* **2002**, *9*, 544–552. [[CrossRef](#)]
67. Gilboa, R.; Zharkov, D.O.; Golan, G.; Fernandes, A.S.; Gerchman, S.E.; Matz, E.; Kycia, J.H.; Grollman, A.P.; Shoham, G. Structure of formamidopyrimidine-DNA glycosylase covalently complexed to DNA. *J. Biol. Chem.* **2002**, *277*, 19811–19816. [[CrossRef](#)]
68. Duclos, S.; Aller, P.; Jaruga, P.; Dizdaroglu, M.; Wallace, S.S.; Doublé, S. Structural and biochemical studies of a plant formamidopyrimidine-DNA glycosylase reveal why eukaryotic Fpg glycosylases do not excise 8-oxoguanine. *DNA Repair* **2012**, *11*, 714–725. [[CrossRef](#)]
69. Eckenroth, B.E.; Cao, V.B.; Averill, A.M.; Dragon, J.A.; Doublé, S. Unique structural features of mammalian NEIL2 DNA glycosylase prime its activity for diverse DNA substrates and environments. *Structure* **2021**, *29*, 29–42.e24. [[CrossRef](#)]
70. Prakash, A.; Eckenroth, B.E.; Averill, A.M.; Imamura, K.; Wallace, S.S.; Doublé, S. Structural investigation of a viral ortholog of human NEIL2/3 DNA glycosylases. *DNA Repair* **2013**, *12*, 1062–1071. [[CrossRef](#)]
71. Golan, G.; Zharkov, D.O.; Feinberg, H.; Fernandes, A.S.; Zaika, E.I.; Kycia, J.H.; Grollman, A.P.; Shoham, G. Structure of the uncomplexed DNA repair enzyme endonuclease VIII indicates significant interdomain flexibility. *Nucleic Acids Res.* **2005**, *33*, 5006–5016. [[CrossRef](#)]
72. Zhdanova, P.V.; Ishchenko, A.A.; Chernonosov, A.A.; Zharkov, D.O.; Koval, V.V. Dynamics and conformational changes in human NEIL2 DNA glycosylase analyzed by hydrogen/deuterium exchange mass spectrometry. *J. Mol. Biol.* **2022**, *434*, 167334. [[CrossRef](#)]
73. Doublé, S.; Bandaru, V.; Bond, J.P.; Wallace, S.S. The crystal structure of human endonuclease VIII-like 1 (NEIL1) reveals a zincless finger motif required for glycosylase activity. *Proc. Natl. Acad. Sci. USA* **2004**, *101*, 10284–10289. [[CrossRef](#)] [[PubMed](#)]

74. Landová, B.; Šilhán, J. Conformational changes of DNA repair glycosylase MutM triggered by DNA binding. *FEBS Lett.* **2020**, *594*, 3032–3044. [[CrossRef](#)] [[PubMed](#)]
75. Sugahara, M.; Mikawa, T.; Kumasaka, T.; Yamamoto, M.; Kato, R.; Fukuyama, K.; Inoue, Y.; Kuramitsu, S. Crystal structure of a repair enzyme of oxidatively damaged DNA, MutM (Fpg), from an extreme thermophile, *Thermus thermophilus* HB8. *EMBO J.* **2000**, *19*, 3857–3869. [[CrossRef](#)] [[PubMed](#)]
76. Gruskin, E.A.; Lloyd, R.S. Molecular analysis of plasmid DNA repair within ultraviolet-irradiated *Escherichia coli*. I. T4 endonuclease V-initiated excision repair. *J. Biol. Chem.* **1988**, *263*, 12728–12737. [[CrossRef](#)]
77. Esadze, A.; Rodriguez, G.; Weiser, B.P.; Cole, P.A.; Stivers, J.T. Measurement of nanoscale DNA translocation by uracil DNA glycosylase in human cells. *Nucleic Acids Res.* **2017**, *45*, 12413–12424. [[CrossRef](#)] [[PubMed](#)]